Quasifission processes in ^{40,48}Ca+^{144,154}Sm reactions

G. N. Knyazheva, E. M. Kozulin, R. N. Sagaidak, A. Yu. Chizhov, M. G. Itkis, N. A. Kondratiev, and V. M. Voskressensky
Flerov Laboratory of Nuclear Reactions, Joint Institute for Nuclear Research, RU-141980 Dubna, Moscow region, Russia

A. M. Stefanini, B. R. Behera, L. Corradi, E. Fioretto, A. Gadea, A. Latina, and S. Szilner*
Istituto Nazionale di Fisica Nucleare, Laboratori Nazionali di Legnaro, I-35020 Legnaro, Padova, Italy

M. Trotta
Istituto Nazionale di Fisica Nucleare, Sezione di Napoli, I-80126 Napoli, Italy

S. Beghini, G. Montagnoli, and F. Scarlassara
Dipartimento di Fisica and INFN-Sezione di Padova, Università di Padova, I-35131 Padova, Italy

F. Haas and N. Rowley
IReS, UMR7500, IN2P3-CNRS/Université Louis Pasteur, BP28, F-67037, Strasbourg Cedex 2, France

P. R. S. Gomes
Instituto de Física, Universidade Federal Fluminense, Av. Litoranea s/n, 24210-340 Niteroi, Brazil

A. Szanto de Toledo
Instituto de Fisica, Universidade de São Paulo, CP 66318, 05315-970 São Paulo, Brazil
(Received 7 February 2007; published 4 June 2007)

Mass-energy and angular distributions of fission fragments for the ^{48}Ca+^{144,154}Sm $\rightarrow$ ^{192,202}Pb, ^{40}Ca + ^{154}Sm $\rightarrow$ ^{194}Pb reactions have been measured. Fusion suppression and the presence of quasifission at energies near and below the Coulomb barrier have been observed for the reactions with the deformed target ^{154}Sm. In the case of the spherical ^{144}Sm target no evidence of quasifission has been found. Quasifission cross sections have been extracted from total fission-like events by analysis of their mass and angular distributions.

DOI: 10.1103/PhysRevC.75.064602 PACS number(s): 25.70.Gh, 25.70.Jj

I. INTRODUCTION

The complete fusion of two massive nuclei is a complex process whose understanding implies a detailed study of the decay products of the compound nucleus (CN), such as CN fission fragments and evaporation residues (ER), and of the products of reactions competing with fusion, such as fission-like fragments produced in quasifission (QF) and deep-inelastic processes. The competition between QF and complete fusion is influenced by the properties of the dinuclear system at contact configuration, where entrance-channel effects play the major role in the reaction dynamics. A decrease in the entrance-channel mass-asymmetry along with an increase in CN-fissility are responsible for the appearance of QF manifested in the suppression of the fusion cross section for combinations leading to strongly fissile compound nuclei [1–4]. Another circumstance that influences the fusion probability is the relative orientation of deformed nuclei, which changes the Coulomb barrier and the distance between the centers of the colliding nuclei. When two interacting nuclei touch each other by their lateral surfaces (near-side collisions), a high formation probability of a spherical CN is expected, whereas in the elongated configuration, when nuclei touch each other by their poles (near-tip collisions), a high QF probability is expected [5,6].

In asymmetric reactions leading to moderately fissile compound nuclei, such as ^{216}Ra*, for which yields of fission and ER production are comparable, QF is manifested in the suppression of the ER production with respect to less asymmetric combinations at energies above the Coulomb barrier [7]. This was observed by comparing reduced ER cross sections for reactions induced by ^{19}F and ^{30}Si with those induced by ^{12}C (the most asymmetric combination leading to ^{216}Ra*). In the more symmetric combination, e.g., with ^{48}Ca, QF is manifested in the mass-energy distributions of fission fragments [8] along with a stronger suppression of ER production [9]. In that case, the contribution of the QF component, corresponding to an asymmetric mass division into the total mass-energy distribution of fission fragments, is estimated as $\sim$30% [8]. At the same time, the ER cross sections indicate a 70% suppression of the CN formation [9]. The apparent discrepancy might be due to a strong peaking of the QF mass-asymmetric component in the forward (backward) direction, which was observed later on [10] and had to be taken into account in the extraction of the CN-fission component

*Ruder Bošković Institute, HR-10002 Zagreb, Croatia.

from the mass-energy and angular distributions of fission fragments. Such peaking is clearly observed in combinations with massive nuclei (leading to the formation of strongly fissile compound nuclei), where the QF process dominates over other reaction channels [11–13]. In these cases a strong QF component is observed in reactions between spherical nuclei [11,12] as well as between spherical projectiles and deformed targets [13].

The question arises, when QF is starting up to appear in reactions with less fissile CN, i.e., where is the onset of QF competition with CN formation, and what is the conditions in the entrance channel, such as the mass-asymmetry, deformation, and neutron excess, which lead to the appearance of QF. In our recent paper [14], we found about 40% fusion suppression in the reaction of ^{48}Ca with the well deformed ^{154}Sm in the energy range from the Coulomb barrier up to the energy corresponding to $E^*_{CN} \simeq 80$ MeV. This follows from the comparison to the ER cross sections obtained in the very asymmetric ^{16}O+^{186}W combination [15,16] leading to the same ^{202}Pb* CN. Note that ER and fission excitation functions obtained in the more asymmetric reaction of ^{30}Si with the deformed ^{170}Er [17], which leads to the neighbor ^{200}Pb* CN, does not show up any fusion suppression [19].

This paper presents the results of fission studies in the reactions ^{16}O+^{186}W and ^{40,48}Ca+^{144,154}Sm at energies close to the Coulomb barrier [20]. The first reaction was chosen as a reference for pure CN-fission, whereas in the second group of reactions we aimed at studying the effects of the entrance-channel mass-asymmetry, target nucleus deformation and neutron excess of the projectile on the competition between fusion-fission and quasifission. Some relevant properties of the system studied are listed in Table I. The mass-angular distributions at two energies around the Coulomb barrier were measured in the reactions ^{48}Ca+^{144,154}Sm, in order to clarify the origin of fission events (CN-fission against quasifission). Detailed CN-fission and QF excitation functions were also obtained for the ^{48}Ca+^{154}Sm system. They are discussed together with the ER cross sections measured earlier.

The paper is organized as follows. The experimental procedure and data analysis are described in Sec. II. The experimental results on the mass-energy and mass-angular distributions, excitation functions for CN-fission and quasi-fission are presented and discussed in Sec. III. Finally, Sec. IV is a summary of the work.

II. EXPERIMENT

The experiments were carried out using ion beams from the XTU Tandem + ALPI accelerator complex of the Laboratori Nazionali di Legnaro (LNL) in the energy ranges 76–132 MeV for ^{16}O (intensity about 10 pnA) and 163–252 MeV for Ca beams (intensity 2–5 pnA). The targets were metal evaporations of enriched isotopes ^{144,154}Sm (with enrichment 96.5%, 98.7% and thickness 50, 200 μg/cm^2, depending on the run) and of $^{186}WO_3$ (with enrichment 97.5% and thickness 50 μg/cm^2) onto thin carbon backings (15–20 μg/cm^2). The thinner Sm targets were mainly used for the fission and ER excitation function measurements [14], whereas with the thicker ones the fission-fragment mass-energy distributions were studied. The targets were installed in the center of a ø = 100 cm scattering chamber facing the beam direction. The beam energy losses in the carbon backing and target layer were about 0.07 MeV for the $^{186}WO_3$ and 0.4 MeV for the thin Sm targets or 2 MeV for the thick ones. This was taken into account in the data analysis. Four silicon surface-barrier detectors were installed on a ring (see Fig. 1) to monitor continuously the beam intensity and position. They detected Rutherford scattering from the target and were placed above and below, and to the left and right of the beam at the same scattering angle $\vartheta_{lab} = 13^\circ$ or 16°, depending on the run. Small correction to the measured cross sections were made according to observed variations in the relative yields of scattered particles in the monitors, due to small changes of beam focusing and position from run to run.

Mass-energy distributions of binary reaction events were measured using the two-arm time-of-flight (TOF-TOF) spectrometer CORSET [24], previously used in studies of heavy-ion induced fission [8,9,25]. It consisted of the compact start detectors designated as St4 and St5 in Fig. 1 and the position-sensitive stop detectors (Sp4 and Sp5 in Fig. 1). The arms of the spectrometer were installed at the same angle

TABLE I. Properties of the systems studied in this work, which lead to the Pb compound nuclei. B_{Bass} is the nominal fusion barrier in the center-of-mass system [20]. β is the deformation parameter for the projectile and target nuclei, as deduced from the electric quadrupole transition probability between the 0^+ ground state and the first 2^+ state [21]. $\alpha = (A_t - A_p)/(A_t + A_p)$ is the entrance-channel mass-asymmetry. A_{CN} is the CN atomic mass number. x_{LD} is the liquid drop fissility parameter (see, e.g., Ref. [22]). $I_{B_f=0}$ is the critical angular momentum for which the fission barrier goes to zero [22]. $B_f(I=0)$ is the fission barrier for zero angular momentum [22]. TKE^{sym} is the total kinetic energy expected for symmetric fission [23].

Reaction	Entrance channel				CN system				
	B_{Bass}	β deformation		α	A_{CN}	x_{LD}	$I_{B_f=0}$	$B_f(I=0)$	TKE^{sym}
	(MeV)	projectile	target				($\hbar$)	(MeV)	(MeV)
^{16}O+^{186}W	69.9		0.226	0.842	202	0.698	79	12.4	143.6
^{48}Ca+^{154}Sm	137.0	0.106	0.341	0.525	202	0.698	79	12.4	143.6
^{40}Ca+^{154}Sm	141.0		0.341	0.588	194	0.712	74	10.9	145.4
^{48}Ca+^{144}Sm	140.0	0.106	0.087	0.500	192	0.715	72	10.4	145.9

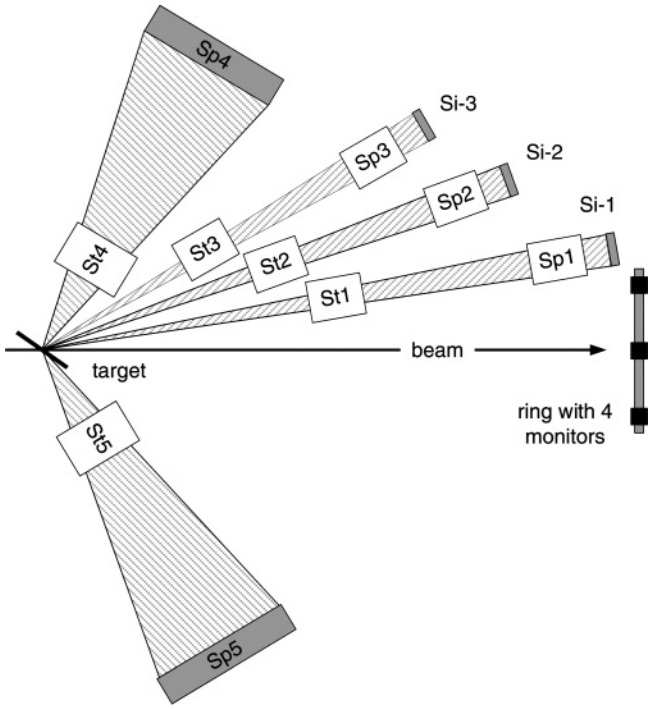

FIG. 1. Sketch of the experimental set-up for measurements of the mass-energy and mass-angular distributions of binary reaction products. See explanations in the text.

60° with respect to the beam direction for the Ca + Sm reactions and at 36.5° and 117.5° for the O + W reaction that corresponds roughly to the opening angle 180° of fragments in the center-of-mass system. The distance between start and stop detectors was 15 cm. Start detectors were placed at a distance of 5 cm from the target. The angular acceptance for both arms was 25° in-plane and ±10° out-of-plane. A typical mass resolution of the spectrometer is about 2–3 amu. The efficiency of the detection for each arm was determined with an α-source and was about 86%. This value depends mainly on the transparency of the electrostatic mirror of the start detector. The data were analyzed event by event, the mass M and total kinetic energy (TKE) of the fragments being deduced from the measured velocities and positions. Binary events with full momentum transfer were selected using folding correlations corresponding to the double-differential cross sections $\partial^2\sigma/\partial M\partial(\mathrm{TKE})$ [8,25].

In order to measure mass-angular distributions of fission fragments, we installed three additional TOF-E telescopes at the angles of 15°, 25°, and 35° to the beam direction (designated as St1–Sp1–Si-1, St2–Sp2–Si-2 and St3–Sp3–Si-3 in Fig. 1). The distance between start and stop detectors for these arms was 15 cm. The start detector was placed at a distance of 12 cm from the target. In the angular distribution measurements, the target was turned at 35° to the beam line. The angular acceptance of each telescope was ±1.5° and mass resolution was 3–4 amu. The detection efficiency of each arm was also obtained with an α-source and was about 75%.

TABLE II. Energy-dependent characteristics for the reactions studied. $E_{\mathrm{c.m.}}$ is the energy in the center-of-mass system. E^*_{CN} is the CN excitation energy calculated with the ground-sate masses [26]. $\langle I\rangle_{\mathrm{CN}}$ is the CN mean angular momentum calculated with the CCFULL code [27]. T_{sad} is the saddle point temperature calculated according to Eq. (3). T_{sci} is the scission point temperature calculated according to Eq. (4).

Reaction	$E_{\mathrm{c.m.}}$ (MeV)	E^*_{CN} (MeV)	$\langle I\rangle_{\mathrm{CN}}$ ($\hbar$)	T_{sad} (MeV)	T_{sci} (MeV)
^{16}O+^{186}W	69.5	48	12	0.89	0.90
	100.4	79	33	1.15	1.14
	111.0	90	38	1.21	1.20
	121.1	100	44	1.30	1.25
^{48}Ca+^{154}Sm	138.8	49	32	0.89	0.87
	147.8	57	37	0.96	0.94
	154.0	63	44	1.01	0.97
	185.3	95	68	1.33	1.10
^{40}Ca+^{154}Sm	138.9	56	27	1.05	1.16
	142.9	60	31	1.10	1.18
	153.2	70	40	1.18	1.23
	158.0	75	48	1.18	1.24
^{48}Ca+^{144}Sm	141.0	38	19	0.77	0.78
	151.5	48	35	0.89	0.86
	167.3	64	52	0.92	0.95

III. EXPERIMENTAL RESULTS AND DISCUSSION

A. Mass-energy distributions

Mass-energy distributions (MED) of fission fragments for the reactions listed in Table I have been measured in the energy range from about the nominal fusion barrier [20] to well above it. Table II contains the values of the CN excitation energy, at which MED are shown in Figs. 2–5 and some relevant energy-dependent characteristics for these reactions. Figures 2–5 display the obtained distributions for fission fragments, namely (from top to bottom): the two-dimensional matrix of counts as a function of the mass and total kinetic energy $N(M,\mathrm{TKE})$; the mass distribution (MD) for fission events framed into the contour line drawn on the two-dimensional mass-energy plot; the mean total kinetic energy $\langle\mathrm{TKE}\rangle$ of fission fragments framed into the same contour line as a function of the fragment mass.

Figure 2 shows the obtained distributions for the ^{16}O+^{186}W reaction. The typical triangular shape of the matrices and the gaussian form of the MD indicate that the manifestation of shell effects in fission is small at the excitation energies investigated for this CN. Namely this type of MD is predicted by the liquid-drop [28] and diffusion models [29] in the case of relatively hot compound nuclei. For such nuclei the variance of MD for fission fragments depends on the excitation energy and angular momentum of the CN. Variances of mass distributions obtained in the ^{16}O+^{186}W reaction will be discussed in the next section (Sec. III B).

The total kinetic energy of fission fragments is mainly determined by the Coulomb repulsion of two deformed fragments at scission point. In the frame of the liquid-drop

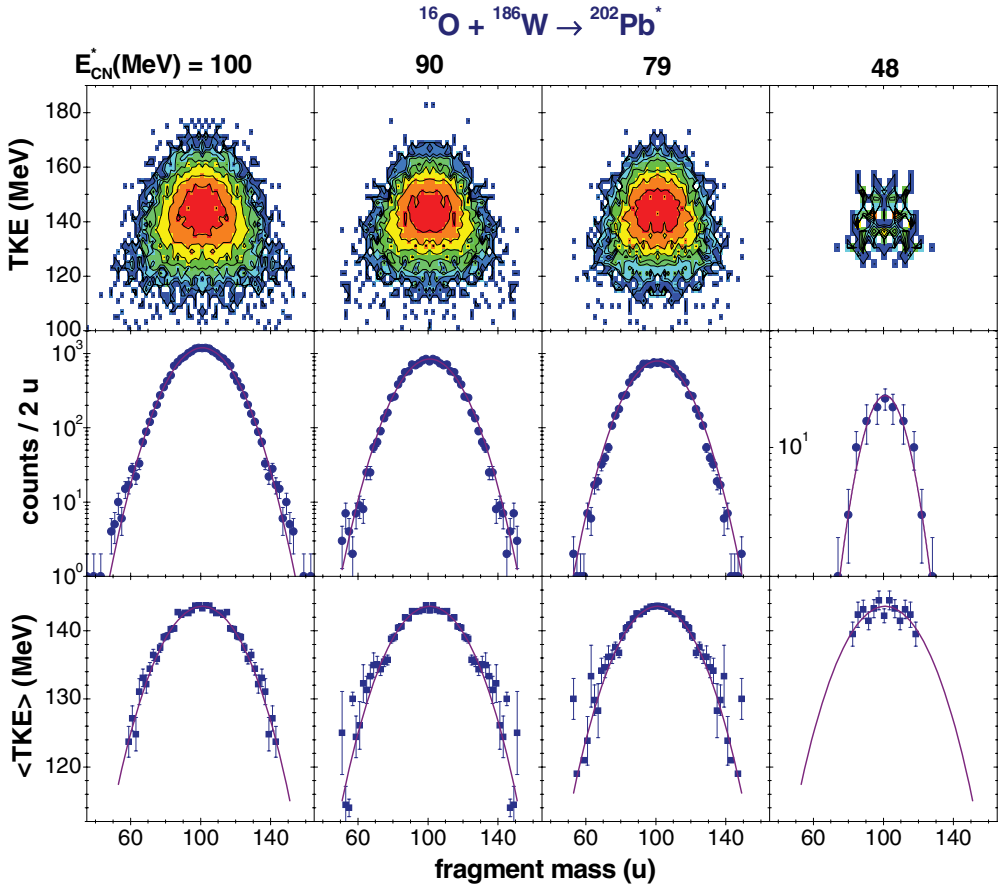

FIG. 2. (Color online) Two-dimensional TKE–mass matrices (upper panels), yields of fragments and their ⟨TKE⟩ as a function of the fragment mass (middle and bottom panels, respectively) in the $^{16}O+^{186}W$ reaction at the different CN excitation energies (designated above upper panels). Solid lines in the middle and bottom panels are Gaussian and parabola fits to the mass and ⟨TKE⟩ distributions, respectively.

model ⟨TKE⟩ has a parabolic dependence on fragment masses and does not vary with the CN excitation energy and angular momentum. The solid line in the bottom panels of Fig. 2 is the parabolic function corresponding to the Viola systematics [23].

So, in the case of the $^{16}O+^{186}W$ reaction, there are no peculiarities in the mass-energy distributions at various energies, i.e., we observe a typical picture of CN-fission in agreement with our expectations for the excited $^{202}Pb^*$.

Figure 3 shows the same quantities for the $^{48}Ca+^{154}Sm$ reaction leading to the same CN. The distributions at the low excitation energies differ significantly from those observed for $^{16}O+^{186}W$. In Fig. 3 (upper panels), the reaction products having masses close to those of projectile and target are identified as quasielastic and deep-inelastic events in the $N(M, \mathrm{TKE})$ matrix, and we will not consider them. Reaction products in the mass range $\simeq$ 55–145 can be identified as totally relaxed events, i.e., as fission (or fission-like) fragments. We have outlined them by solid lines in the panels. Henceforth we consider the properties of only these events. Their mass distributions show the relatively large contribution ($\simeq$ 30% at the lowest energy) of the "asymmetric fission mode", appearing as "shoulders" peaked around masses 65 and 140, at $E^*_{CN} = 49$ and 57 MeV. We notice that such "shoulders" are indistinguishable at higher excitation energies. The symmetric fission component is described by a Gaussian whose variance is larger than the one obtained for the ^{16}O reaction at the same excitation energy (this circumstance will be discussed in the next section (Sec. III B). The shape of the curves obtained for ⟨TKE⟩ at $E^*_{CN} = 49$ and 57 MeV (bottom panels in Fig. 3) is far from a parabolic one, if we compare these curves with the parabolas fitted to the $^{16}O+^{186}W$ ⟨TKE⟩ data (see bottom panels in Fig. 2).

A similar picture is observed in the case of the $^{40}Ca+^{154}Sm$ reaction, i.e., noticeable mass "asymmetric shoulders" are visible (less pronouncedly) at the energies around the nominal fusion barrier [20] at $E^*_{CN} = 56$ and 60 MeV, as one can see in Fig. 4 (middle panels). The contribution of this "asymmetric shoulders" to all fission-like events (outlined by the corresponding octagons in the upper panels of the figure) is about 10% at these energies. It decreases with increasing the ^{40}Ca energy, and almost disappears at the highest energy ($E^*_{CN} = 75$ MeV). The ⟨TKE⟩ corresponding to the symmetric mass division is close to the one given by systematics [23] (see Table I). The lack of similar data for a very asymmetric combination leading to the same $^{194}Pb^*$ CN does not allow further considerations.

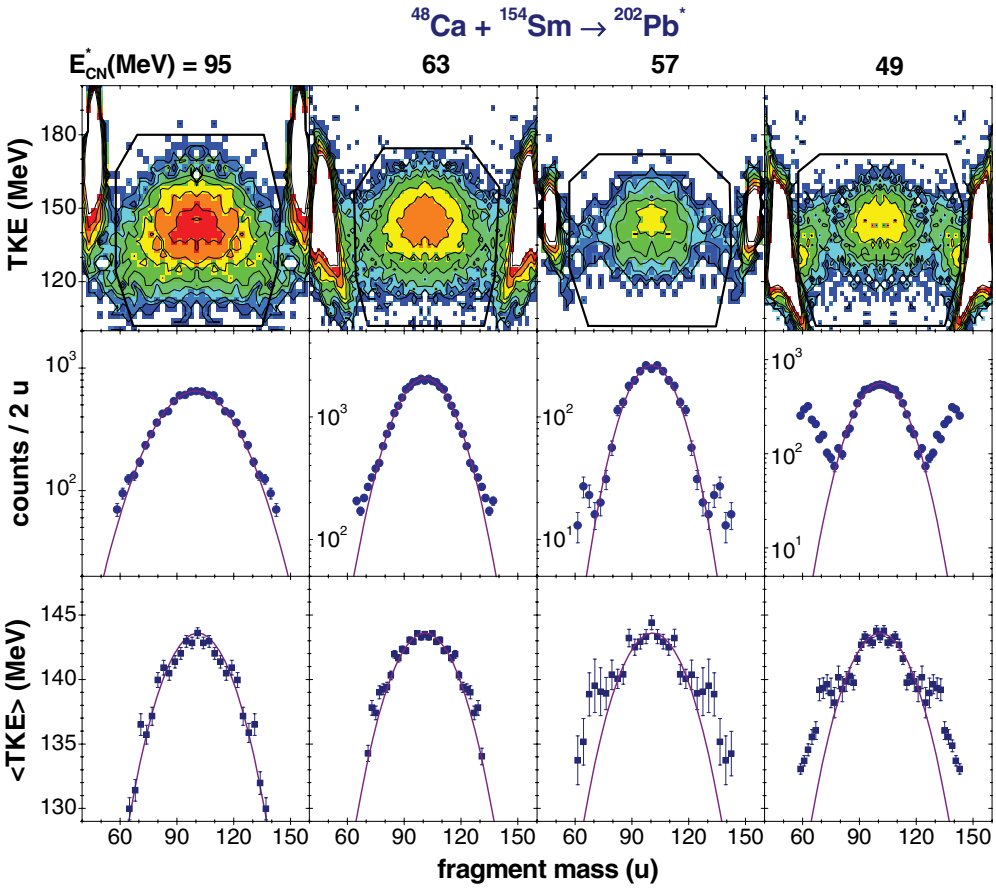

FIG. 3. (Color online) The same as in Fig. 2 but for the reaction ^{48}Ca+^{154}Sm. In the bottom panels parabola fits obtained for ⟨TKE⟩ in ^{16}O+^{186}W at the same excitation energies are shown for comparison (solid lines).

A quite different picture is observed for MED obtained for the ^{48}Ca+^{144}Sm reaction. We do not observe any hint of the "asymmetric shoulders" at $E^*_{CN} = 48$ MeV, i.e., at about the same excitation energy at which they were observed in the case of the ^{48}Ca+^{154}Sm reaction ($E^*_{CN} = 49$ MeV). These "asymmetric shoulders" do not show up at the lower and higher CN excitation energies, as one can see in Fig. 5 (middle panels). As in the previous case, ⟨TKE⟩ corresponding to the symmetric mass division is close to the one given by systematics [23] (see Table I). The main differences of this reaction comparing with the two previous ones (induced on the strongly deformed ^{154}Sm nucleus) are a very small target deformation and a lower value of the entrance-channel mass asymmetry (see Table I). As we can see, the latter does not affect complete fusion, and one can state that, in the case of the ^{48}Ca+^{144}Sm reaction with two almost spherical nuclei at energies above the fusion barrier, we mainly observe pure CN-fission of ^{192}Pb*.

Coming back to the ^{16}O+^{186}W and ^{48}Ca+^{154}Sm systems leading to the ^{202}Pb* CN, one can notice that the picture resembles the one observed in our previous study of the ^{12}C+^{204}Pb and ^{48}Ca+^{168}Er systems leading to the more fissile ^{216}Ra* [8]. In that case at $E^*_{CN} \simeq 40$ MeV in both reactions, about 1.5% contribution from asymmetric fission was observed in ^{12}C+^{204}Pb, whereas in the case of ^{48}Ca+^{168}Er this value was about 30%. For reactions leading to ^{202}Pb*, we could not observe an asymmetric fission component in the ^{16}O+^{186}W reaction at the lowest $E^*_{CN} = 48$ MeV. This is mainly due to poor statistics caused by low fissility of the CN and a relatively small fusion cross section at this energy. The CN produced in the ^{48}Ca+^{154}Sm reaction at the same excitation energy has a higher fission probability that is mainly connected with higher angular momenta brought in by the heavier projectile. At first sight, this allowed us to observe not only a "normal" symmetric fission component, but also an asymmetric one produced with a yield of about 30% of all fission events. We put aside the origin of this component here. In the framework of normal fission, which follows the formation of a CN, it is difficult to understand our observations, since it is well known that increasing the angular momentum the manifestation of shell effects decreases [30]. In the case of a massive projectile such as ^{48}Ca, with respect to the ^{16}O reaction, the most plausible explanation is a large contribution from quasi-fission into the asymmetric component, a process bypassing the usual CN stage. This conclusion is supported by similar results of our previous experiments [8,9] and by the mass-angular distributions measured in the present work (see Sec. III C). Another possibility that can shed light upon a presence of QF events in MED is the analysis of widths of the mass distributions. One cannot exclude a partial mass equilibration during the QF process, which can lead to nearly symmetric

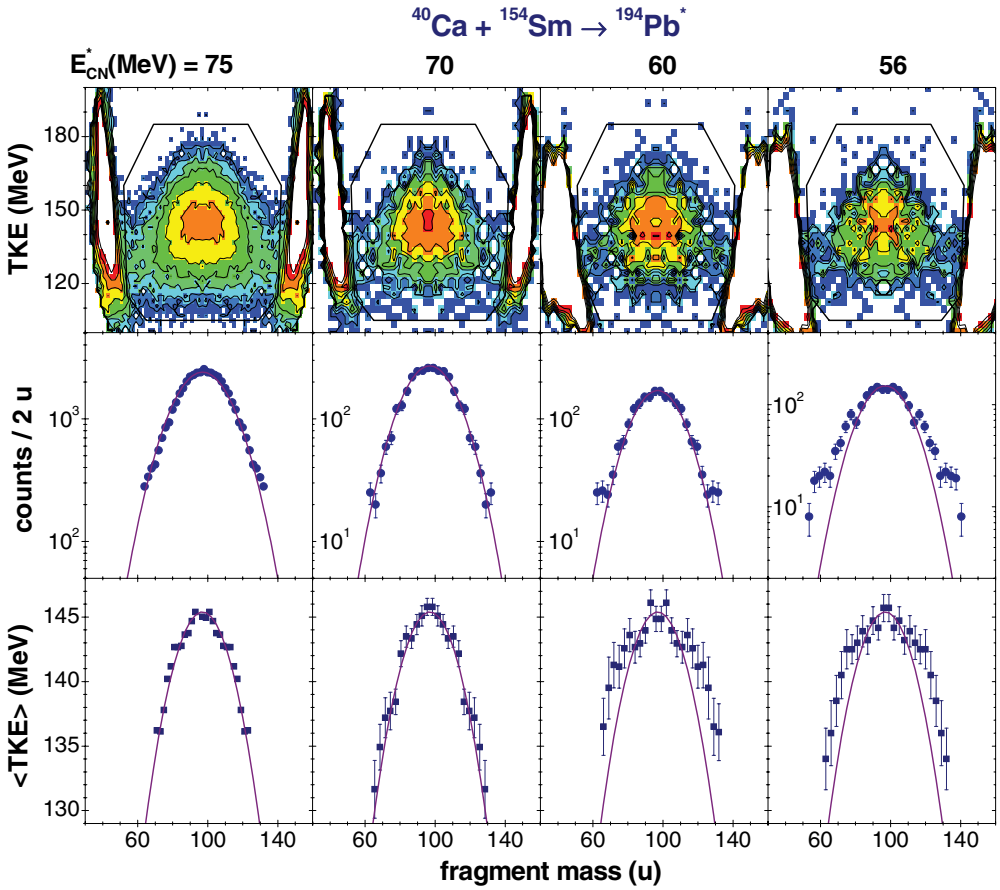

FIG. 4. (Color online) The same as in Fig. 2 but for the reaction ^{40}Ca+^{154}Sm.

fission of a composite system and could affect the symmetric mass distributions of true CN-fission.

B. Variances of mass distributions in ^{16}O+^{186}W and ^{48}Ca+^{154}Sm

As we mentioned above, the width of the fission fragment mass distribution could be an indicator of the presence of QF in fission-like mass spectra. A strong increase in the width of mass distributions is observed with reactions leading to strongly fissile compound nuclei in going from quite asymmetric to less asymmetric combinations [4,13]. In the case of reactions leading to less fissile compound nuclei, an increase in the width of mass distributions for less asymmetric systems [7] is not necessarily connected with the manifestation of QF, but could be due to the larger angular momentum brought in by heavier projectiles [31].

In general, the width of the mass distribution depends on the excitation energy and angular momentum of a CN. In the first approximation [32], the variance σ_M^2 increases linearly with $\langle I^2\rangle$ and with the nuclear temperature T, and can be written as

$$\sigma_M^2 = \frac{\partial\sigma_M^2}{\partial T}T + \frac{\partial\sigma_M^2}{\partial\langle I^2\rangle}\langle I^2\rangle. \qquad (1)$$

The first term in Eq. (1) corresponds to the variance of the mass distribution at zero angular momentum and can be calculated (with some assumptions) as

$$\sigma_M^2 = \frac{A_{\rm CN}^2 T}{16}\left[\left(\frac{d^2V}{d\eta^2}\right)_{\eta=0}\right]^{-1}, \qquad (2)$$

where $(\frac{d^2V}{d\eta^2})_{\eta=0}$ is the stiffness of a nucleus for symmetric mass division ($\eta = 0$) and at zero angular momentum, which is taken from the corresponding systematics [32] for the assumed temperature (see below). The sensitivity of the variance to the angular momentum is much weaker, although not negligible. For the estimates of the coefficient $\frac{\partial\sigma_M^2}{\partial\langle I^2\rangle}$ we used similar systematics presented in [32].

Estimates of the nuclear temperature depend on an assumption on the point, where properties of fission fragments are determined, namely, at the saddle or at the scission point of the fissioning nucleus. For light nuclei the saddle and the scission point are very close to each other, while for heavy nuclei the descent from the saddle to the scission point has an essential extension. We consider both these cases bearing in mind that the properties of fission fragments might be determined in the path from the saddle to the scission point. The temperature of the nucleus at the saddle point can be estimated (see, e.g., [32]) as

$$T_{\rm sad} = \left[\frac{E^*_{\rm CN} - B_f(I) - E_{\rm pre} - E_{\rm rot}}{a}\right]^{1/2}, \qquad (3)$$

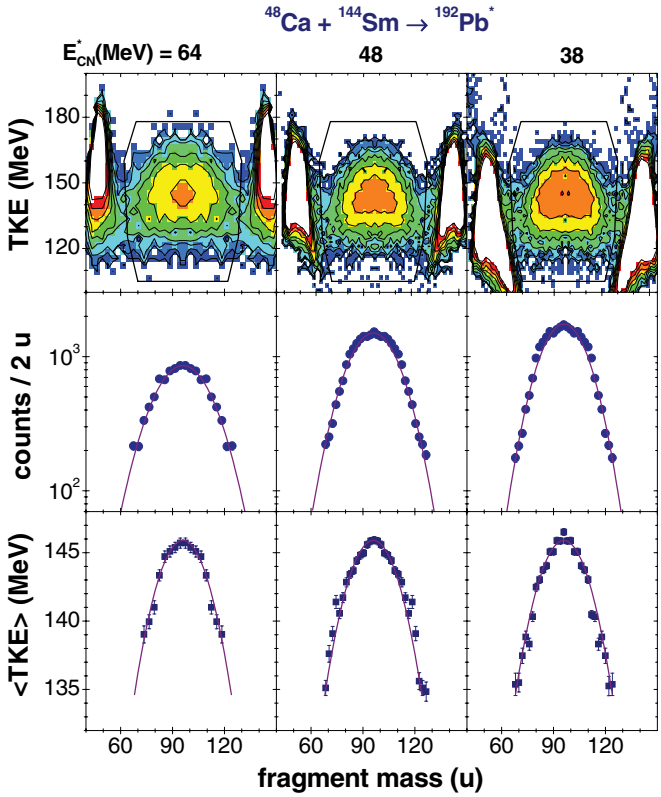

FIG. 5. (Color online) The same as in Fig. 2 but for the reaction ^{48}Ca+^{144}Sm.

where the quantities $E^*_{\rm CN}$ and $B_f(I)$ were defined earlier, $E_{\rm rot}$ is the rotational energy of the CN at the saddle point calculated according to the rotating liquid-drop model [33], $E_{\rm pre}$ is the energy carried out by prefission neutrons, which is estimated with the empirical systematics [32]; and a is the level density parameter. The temperature at the scission point is estimated with the relations (see, e.g., [32])

$$\begin{aligned} E^*_{\rm sci} &= E^*_{\rm CN} + Q_{\rm sym} - {\rm TKE} - E_{\rm pre} - E^{\rm sci}_{\rm rot} - E_{\rm def}, \\ T_{\rm sci} &= (E^*_{\rm sci}/a)^{1/2}, \end{aligned} \tag{4}$$

where $Q_{\rm sym}$ is the reaction Q value for symmetric fission, $E_{\rm def}$ is the deformation energy of fragments, $E^{\rm sci}_{\rm rot}$ is the rotational energy at the scission point, which is estimated according to the prescription considered in [32]. As for the deformation energy, this parameter is strongly model dependent, therefore we assume $E_{\rm def} = 0$ and thus the temperature given by Eq. (4) should be considered as an upper limit. The saddle and scission point temperatures estimated for the systems studied in the present work are listed in Table II. One can see that these temperatures are very similar within the calculation, so we estimate the variances of the mass distributions simply by using the saddle point temperature given by Eqs. (1)–(3), which can be written in the reduced form as

$$\sigma^2_M = (98.1 \pm 15.1)T + (0.05 \pm 0.01)\langle I^2 \rangle. \tag{5}$$

Figure 6 shows the standard deviation of the mass distributions obtained for the ^{16}O+^{186}W reaction at seven energies

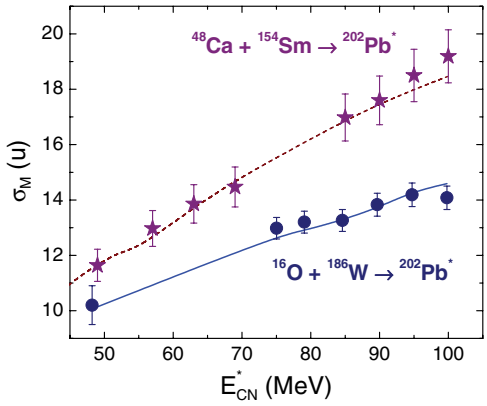

FIG. 6. (Color online) The experimental (symbols) and calculated (lines) variances for fission fragment mass distributions obtained in the reactions ^{16}O+^{186}W and ^{48}Ca+^{154}Sm.

compared with the calculations according to Eq. (1). One can see that the approximation of Eq. (5) reproduces well the experimental variances obtained in the present work. For the ^{48}Ca+^{154}Sm reaction the symmetric fission component is described by a Gaussian with a variance larger than those obtained for the ^{16}O reaction at the same excitation energy. This increase in variance is consistent with the Eq. (5). As we see from Table II, the mean angular momentum of the CN is much larger for ^{48}Ca+^{154}Sm than for ^{16}O+^{186}W at the same excitation energy. Thus the observed increase in σ^2_M for the former, compared to the latter at the same excitation energy, as is shown in Fig. 6, agrees with expectations for normal symmetric fission of the excited ^{202}Pb* CN.

C. Mass-angular distributions for ^{48}Ca+^{144,154}Sm

As it was mentioned in Sec. I, the analysis of the mass-angular distributions of fission fragments allows one to derive the QF component and CN-fission from overall fission-like products detected in an experiment. Following the statistical model considerations [34], the angular distribution of fission fragments for CN-fission in the c.m. system is given by the expression

$$\begin{aligned} W(\theta) = &\sum_{I=0}^{\infty}(2I+1)T_I \sum_{K=-I}^{I}(2I+1)\left|d^I_{0K}(\theta)\right|^2/2 \\ &\times\exp\left[-K^2/2K_0^2(I)\right]\Big/\sum_{K=-I}^{I}\exp\left[-K^2/2K_0^2(I)\right], \end{aligned} \tag{6}$$

where I is the spin of the CN, d^I_{0K} is the symmetric top wave function, K is the projection of the spin I on the symmetry axis, K_0 is the variance of the K distribution and T_I is the transmission coefficient for the I partial wave. Within this model the fission fragment angular distribution depends only on the spin of the compound nucleus via the transmission coefficient T_I and the parameter $K_0 = J_{\rm eff}T/\hbar$, where T is the temperature at the saddle point, $J_{\rm eff}$ is the effective moment of inertia.

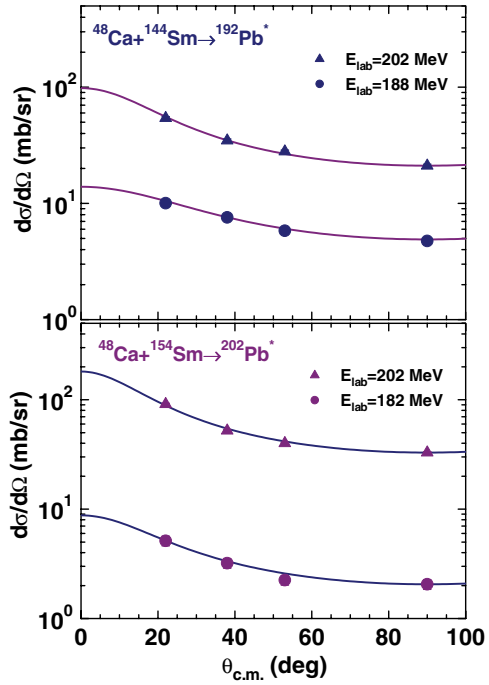

FIG. 7. (Color online) Angular distributions of all fission-like products obtained in the ^{48}Ca+^{144}Sm and ^{48}Ca+^{154}Sm reactions (upper and lower panel, respectively). Symbols are experimental data, solid lines correspond to the calculation with Eq. (6).

Usually it is assumed that quasifission is not an equilibrium process bypassing the CN stage, hence the time scale for QF should be shorter than for true CN fission. In QF, as is also assumed, the saddle point configuration is not reached, and the shape and K equilibration of the intermediate system are different from CN fission. The K-distribution may correspond to a statistical equilibrium of shapes more elongated than the true saddle point or it may be not equilibrated at all. This leads to a large angular anisotropy incompatible with the one observed for CN fission, or to a forward-backward asymmetry of the angular distribution for QF products.

The angular distributions for all fission-like events at two energies near and above the Coulomb barrier, which have been obtained in the ^{48}Ca+^{144}Sm reaction, are shown in Fig. 7 (upper panel). The experimental values of K_0 was found for these distributions by fitting the data with Eq. (6). These K_0 values are in a good agreement with those calculated using the rotating liquid drop model predictions [33] for the fission barrier heights and the moments of inertia.

Angular distributions for different fragment masses were derived attempting to find experimental evidence for the QF nature of the mass-asymmetric "shoulders" observed in ^{48}Ca+^{154}Sm (see Fig. 3). In Figs. 8 and 9 the angular distributions for the selected mass bins of fission-like fragments are shown. The width of each mass bin is 5 amu (mainly determined by statistics and mass resolution). The solid curves are fits to the experimental data given by the expression similar to the one proposed in [13]

$$\frac{d\sigma}{d\theta} = 2\pi \sin\theta \{a + b \exp[\gamma(\theta - \pi/2)]\} W(\theta), \qquad (7)$$

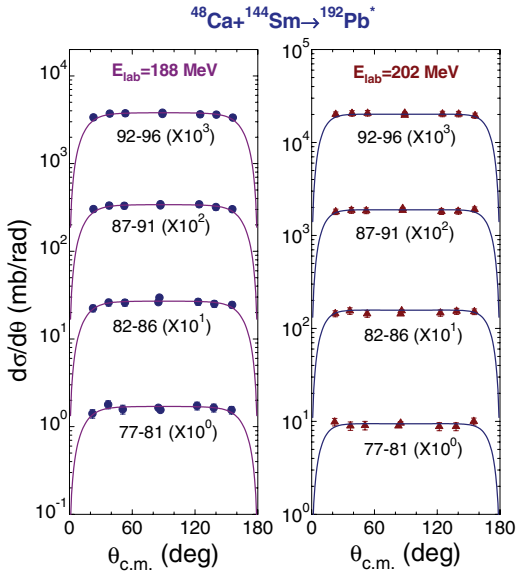

FIG. 8. (Color online) Differential cross sections for fission-like fragments in the reaction ^{48}Ca+^{144}Sm for different fragment mass bins. The solid lines are best fits to the data using Eq. (7).

where $W(\theta)$ is the angular distribution for the CN fission according to Eq. (6), γ is a slope parameter in the exponential decay function reproducing the evident forward-backward asymmetry, and a, b are normalization parameters corresponding to the symmetrical and asymmetrical parts of angular distributions. The value of the slope parameter γ was fixed at -0.02 for all mass bins. Approximately the same value for this parameter was found in [13].

One can see that for the reaction ^{48}Ca+^{144}Sm angular distributions are symmetrical for all selected masses and very well described by Eq. (7) with $b = 0$ and K_0 calculated

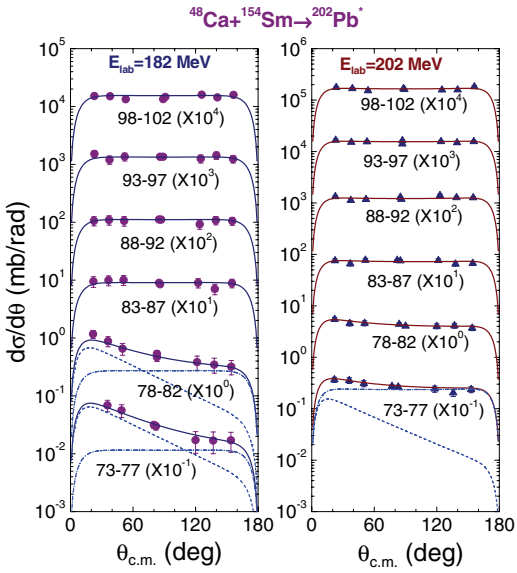

FIG. 9. (Color online) The same as Fig. 8 but for the reaction ^{48}Ca+^{154}Sm. Decompositions of distributions for light masses according to Eq. (7) are shown with dashed and dash-dotted lines (asymmetrical and symmetrical parts, respectively).

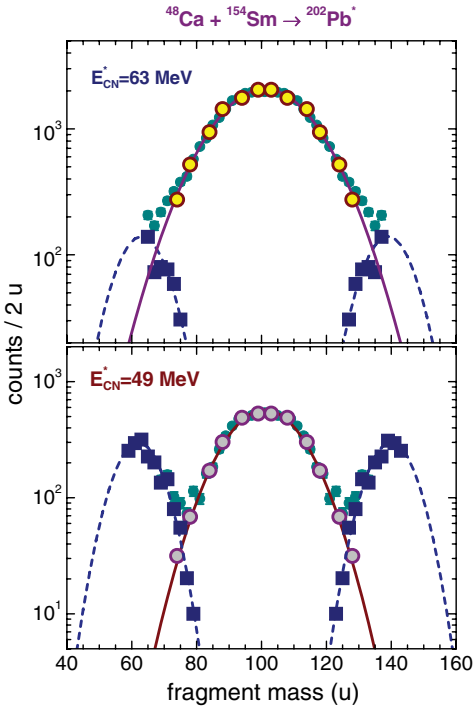

FIG. 10. (Color online) Mass distributions obtained for the ^{48}Ca+^{154}Sm reaction, i.e., the same as in Fig. 3 (small solid circles). Solid lines are Gaussians with variances according to Eq. (5), large open circles correspond to the symmetric part of the mass-angular distributions obtained with Eq. (7), solid squares represent the QF component and dashed lines are the Gaussian fits to the QF component.

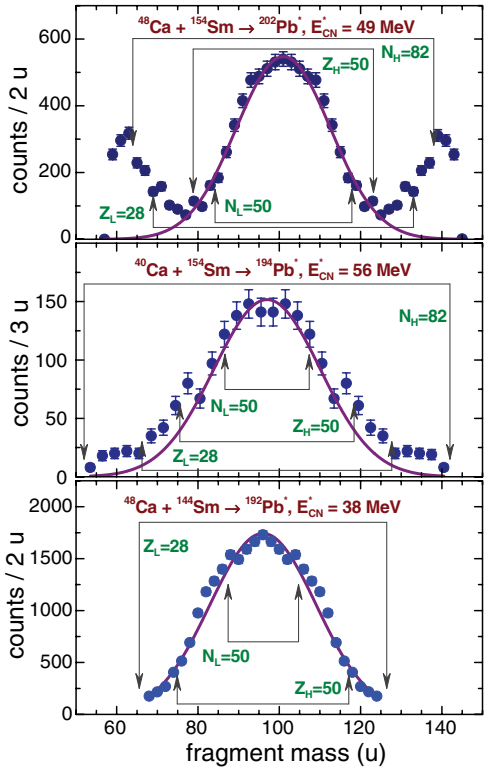

FIG. 11. (Color online) Location of the closed shell (designated by arrows connected with horizontal lines for complementary fragments) in the fragment mass distributions obtained at the lowest CN excitation energies for the three reactions ^{48}Ca+^{154}Sm (upper panel), ^{40}Ca+^{154}Sm (middle panel) and ^{48}Ca+^{144}Sm (bottom panel).

for true CN fission, whereas for the reaction with ^{154}Sm a significant forward-backward asymmetry is observed in the angular distributions displayed for light fragment masses. This forward-backward asymmetry is observed at both energies of ^{48}Ca, but the contribution of the asymmetric-mass portion is larger at the lower energy. We extracted the symmetrical part of the angular distribution corresponding to CN-fission for all mass bins. In Fig. 10 these symmetrical parts of angular distributions are shown by open circles. Solid lines in the figure correspond to the mass distributions that can be described with variance given by Eq. (5), whereas dashed lines correspond to the Gaussian approximation for the asymmetrical mass components. As we see, the symmetrical parts agree very well with calculated mass distribution and these events can be associated with pure CN-fission process, whereas the asymmetric-mass "shoulders" correspond to the pronounced forward-backward asymmetry in angular distributions and these events should be associated with the QF process.

The decomposition in Fig. 10 implies that a part of the QF component is cut off by our contours (see Fig. 3), since it overlaps with deep-inelastic and quasi-elastic events. For more realistic estimates of the QF cross sections (see Sec. III E), we corrected the yields of extracted QF events using the Gaussian fits to the data. This correction increases linearly when decreasing the QF component selected from all fission-like events using the procedure described in Sec. III B.

D. Shell effects in QF

In our previous study [8], the mass distribution for fission-like fragments, which was measured in the ^{48}Ca+^{168}Er reaction at the excitation energy $E^*_{CN} \simeq 40$ MeV, along with a maximum corresponding to the symmetric mass division around $A_{CN}/2$, reveals two additional "asymmetric shoulders" corresponding to QF fragments around the closed shell numbers $Z = 50$ and $N = 50, 82$. In Fig. 11 we show those Ca + Sm fragment mass distributions that correspond to the lowest Pb CN excitation energies, in order to search for the effect of the closed shells in these cases. The arrows in the figure show the positions of the spherical closed shells with $Z = 28, 50$ and $N = 50, 82$ and their complementary masses for light (L) and heavy (H) fragments, which were derived with a simple assumption on N/Z equilibration. In the case of ^{48}Ca+^{154}Sm (upper panel) the major part of the asymmetric component fits into the region of the $Z_L = 28$ and $N_H = 82$ shells, and its maximal yield is close to the latter one. Thus, we have an indication that the shell structure of the fragments formed in the ranges of the light $M_L = 60$–75 and heavy $M_H = 130$–145 masses, respectively, strongly favors the QF process, the shells in both light and heavy fragments playing an important role. In the case of the ^{40}Ca+^{154}Sm reaction leading to the neutron-deficient ^{194}Pb* CN, the closed shells seem to be less effective in the formation of the QF asymmetric component, as one can see in the middle panel of the figure. Finally, for the ^{48}Ca+^{144}Sm reaction, where the asymmetric

component is not observed, the closed shells with $N_H = 50$ and $Z_H = 50$ fall into the region of the symmetric mass distribution, i.e., in the region of "normal" CN-fission (bottom panel in Fig. 11).

The question arises: why do shell effects in the case of the reactions leading to ^{202}Pb* and ^{194}Pb* manifest themselves in the QF process even at relatively high excitation energy ($E^*_{CN} = 49$ and 56 MeV, respectively) but not in the CN fission of ^{192}Pb* even at lower excitation energy ($E^*_{CN} =$ 38 MeV)? This may be explained qualitatively within the concept of the dinuclear system (DNS) [35] (originally elaborated for deep inelastic reactions and then applied to quasifission) or by using a "hybrid" model [36] based on a two-center concept. In these models the potential energy plays an important role and depends on the fragment masses formed in the QF process. The potential energy surface (PES) of a DNS is strongly modulated by shell effects. The minima of the PES lie near the doubly magic numbers that play an important role in the evolution of DNS from the contact point to the CN formation. This evolution corresponds to a strong redistribution of masses of initial nuclei leading to QF. The DNS excitation energy is counted from the valley of PES for each particular mass partition rather than from the ground state of the CN. Since this DNS excitation energy is usually higher than the ground state of the CN, the excitation energy of separated fragments is, on average, lower. Thus calculations of the PES in the framework of the generalized liquid-drop model (GLDM) [37], taking into account the proximity energy [38] and shell corrections [39], lead to a strongly modulated PES and driving potential for fusion leading to ^{216}Ra* [40]. This PES shows a deep local minimum corresponding to the configurations with closed-shell fission-like fragments having $Z = 50$ and $N = 50, 82$, exactly the same that form the "asymmetric shoulders" observed in the ^{48}Ca+^{168}Er reaction [8]. The same result is obtained in the framework of the "hybrid" model [36] (see Ref. [10]). Calculations for ^{202}Pb* [40] show that the fragmentation process leading to the formation of nuclei around $Z_L = 28$ and $N_H = 82$ is about 20 MeV "colder" than the CN formation (leading to CN-fission), and the sensitivity to the shell structure is, therefore, higher than in the case of the CN formation.

E. Cross sections for ^{48}Ca+^{154}Sm

The absolute differential cross sections for all fission-like events observed in the reaction ^{48}Ca+^{154}Sm were measured at the angle $\theta_{c.m.} = 90^\circ$ and at energies from well below to well above the Coulomb barrier. Total cross sections σ_{fis} for all fission-like events were estimated assuming that the angular distribution is proportional to $1/\sin\theta_{c.m.}$. This procedure seemed the most reasonable since detailed angular distributions are not available at present, as well as any model (theory) for the angular distribution of fragments produced in the QF process. The differential cross section for CN fission was derived from the differential cross section of fission-like events by taking into account the width of the mass distribution, as described in Sec. III B. The integral CN-fission cross section σ_{CN-fis} was deduced with angle integration, assuming that the angular distribution is described by Eq. (6). Thus, the integral QF cross section σ_{QF} could be estimated as

$$\sigma_{QF} = \sigma_{fis} - \sigma_{CN-fis}. \quad (8)$$

In the estimate of the QF cross section we took into account a correction due to overlapping of fission-like events with those corresponding to deep-inelastic and quasielastic processes as described at the end of Sec. III C. The absolute cross section values for all fission-like events, CN-fission and QF are presented in Table III. At high energies only upper limits for the QF cross sections were obtained, due to a very low contribution of the process into all fission-like events. At deep sub-barrier energies we could not separate QF and CN fission due to poor statistics collected in experiments.

In Fig. 12 the excitation functions for CN-fission and QF are shown together with ER cross sections measured in the same runs at the same energies [14]. CN fission and ER cross sections allow us to obtain the fusion cross sections as $\sigma_{fus} = \sigma_{ER} + \sigma_{CN-fis}$. These fusion cross sections are close to the capture cross sections presented in [14], which are characterized by a very wide (20–22 MeV) barrier distribution extended down to about 125 MeV [14]. With the present data the barrier distribution for fusion could be obtained. We see that the QF cross section increases with increasing energy up to $E_{c.m.} \simeq 150$ MeV and saturates above it at the level of ~ 40 mb. Note that the barriers for side and tip collisions correspond to 149.7 MeV and 129.1 MeV, respectively, as we estimated with standard parameters of the Woods-Saxon potential [41] and β deformations listed in Table I.

The relative contribution of QF into the capture cross section (the sum of ER, CN fission, and QF cross sections) for the reactions ^{40,48}Ca+^{154}Sm is shown in Fig. 13. We see that this contribution increases with decreasing energy for both reactions, but for ^{48}Ca it is larger than in the case of ^{40}Ca. This observation can be qualitatively explained by the difference in the entrance-channel mass asymmetry α for the reactions in the case of ^{48}Ca and ^{40}Ca ($\alpha = 0.525$ and 0.588, respectively). Such variation in the relative contribution of QF into the capture cross section is in a qualitative agreement with the behavior of the fusion probability as a function of the entrance-channel mass asymmetry, which is based on the comparison of the ER cross sections for different CN systems studied at energies near the Coulomb barrier [19,40]. At the same time one should remind that the QF component, which is responsible for the relatively small fusion suppression at barrier energies, are only observed in the fission study of the reactions with the well deformed ^{154}Sm nucleus (not in the reaction with the spherical ^{144}Sm), in spite of $\alpha(^{144}\text{Sm}) < \alpha(^{154}\text{Sm})$. The last circumstance implies stronger fusion suppression in the case of the reaction with ^{144}Sm, according to the simple liquid-drop model considerations [7,19,37,40].

Considering the effects of the entrance-channel mass asymmetry and deformations on the fusion probability of massive nuclei, one can note that in the framework of dynamical calculations [42] the distortion of nuclear shape due to the Coulomb force is much smaller than the static nuclear deformation. The rotation angle of the deformed target nucleus induced by the Coulomb interaction during the approaching

TABLE III. Cross section values obtained in the reaction ^{48}Ca+^{154}Sm at different energies in the c.m. system ($E_{\text{c.m.}}$). σ_{fis} is cross section of all fission-like events, $\sigma_{\text{CN-fis}}$ is the CN-fission cross section and σ_{QF} is the QF cross section.

$E_{\text{c.m.}}$ (MeV)	σ_{fis} (mb)	$\sigma_{\text{CN-fis}}$ (mb)	σ_{QF} (mb)
191.12	933 ± 52	878 ± 51	⩽55
186.08	893 ± 51	837 ± 50	⩽55
181.12	844 ± 48	785 ± 46	⩽59
176.07	793 ± 45	733 ± 44	⩽60
158.16	501 ± 24	460 ± 23	41 ± 33
156.33	427 ± 21	390 ± 21	37 ± 29
154.50	340 ± 16	302 ± 16	38 ± 23
152.67	298 ± 14	258 ± 14	40 ± 20
150.84	242 ± 12	207 ± 12	35 ± 16
149.01	162 ± 8	136 ± 8	26 ± 11
148.40	163 ± 8	134 ± 7	28 ± 11
147.79	152 ± 7	123 ± 7	29 ± 10
147.18	137 ± 7	110 ± 6	28 ± 9
146.56	132 ± 6	104 ± 6	29 ± 9
145.95	115 ± 6	88.1 ± 5	27 ± 8
145.34	102 ± 5.0	77.0 ± 4.5	25.5 ± 6.7
144.73	89.9 ± 4.3	66.1 ± 3.8	23.8 ± 5.8
144.12	78.3 ± 3.8	56.3 ± 3.3	22.0 ± 5.0
143.51	75.0 ± 3.6	52.5 ± 3.1	22.5 ± 4.8
142.90	65.1 ± 3.1	44.4 ± 2.6	20.7 ± 4.1
142.29	53.8 ± 2.6	35.7 ± 2.2	18.1 ± 3.4
141.68	44.8 ± 2.2	28.8 ± 1.8	16.0 ± 2.8
141.07	39.7 ± 1.9	24.7 ± 1.5	15.0 ± 2.5
140.46	34.2 ± 1.6	20.5 ± 1.3	13.7 ± 2.1
139.85	31.8 ± 1.5	18.4 ± 1.1	13.5 ± 1.9
139.23	26.0 ± 1.2	14.4 ± 0.8	11.6 ± 1.5
138.62	22.0 ± 1.1	11.6 ± 0.9	10.3 ± 1.4
138.01	18.4 ± 0.9	9.2 ± 0.8	9.1 ± 1.2
137.40	16.6 ± 0.8	7.9 ± 0.7	8.8 ± 1.1
136.79	14.0 ± 0.7	6.3 ± 0.6	7.7 ± 0.9
136.18	10.1 ± 0.5	4.3 ± 0.4	5.8 ± 0.7
135.57	8.37 ± 0.4	3.3 ± 0.3	5.1 ± 0.5
134.96	7.31 ± 0.4	2.7 ± 0.3	4.6 ± 0.5
134.35	5.94 ± 0.3	2.0 ± 0.2	3.9 ± 0.4
133.74	4.45 ± 0.3		
133.13	2.44 ± 0.2		
132.52	2.40 ± 0.3		
131.91	1.55 ± 0.2		
131.30	1.02 ± 0.2		
130.69	0.81 ± 0.14		
130.08	0.40 ± 0.08		
129.47	0.42 ± 0.08		
128.86	0.17 ± 0.05		

process was found also to be small (3°–5°) [42]. So, the onset of QF in the studied reactions might be explained by target deformation. The fusion probability is reduced at the near-tip collisions below the nominal fusion (Bass) barrier and QF shows up. The near-side collisions at these low energies lead to small fusion probability due to a higher value of the fusion barrier. At above-barrier energies all target orientations

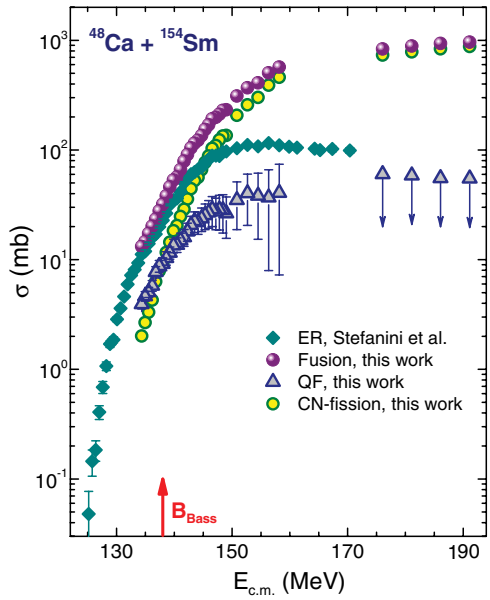

FIG. 12. (Color online) Fusion cross sections (as the sum of CN-fission and ER [14]) in comparison with QF cross sections obtained for the ^{48}Ca+^{154}Sm reaction.

contribute and near-side collisions mainly determine the CN formation. Qualitatively, this consideration corresponds to the model proposed for the explanation of a high angular anisotropy of fission fragments, which is observed in reactions leading to strongly fissile compound nuclei [5,6]

Comparing the mean value of the fusion probability obtained with the fission study in ^{48}Ca+^{154}Sm at barrier energies ($P_{\text{fus}} = 0.801 \pm 0.014$ at $E_{\text{c.m.}} = B_{\text{Bass}} \pm 4$ MeV), and the probability deduced from the comparison of ER cross sections obtained in the same reaction and in the very asymmetric ^{16}O+^{186}W one ($P_{\text{fus}} = 0.60 \pm 0.09$ at $E_{\text{c.m.}} \geqslant B_{\text{Bass}}$ [14,19]), we have a difference between these values. Moreover, according to the fission study, the contribution of the QF component decreases with the energy and becomes negligible at energies well above the fusion barrier ($P_{\text{fus}} \geqslant 95\%$ at $E_{\text{c.m.}} - B_{\text{Bass}} \geqslant 25$ MeV). Since the present fission and ER experiments were performed in the same runs

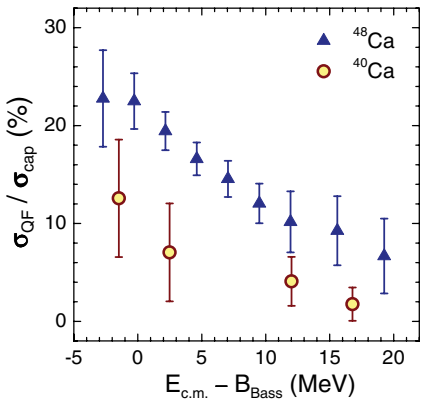

FIG. 13. (Color online) The relative contribution of QF to the capture cross sections for ^{48}Ca+^{154}Sm (filled triangles) and ^{40}Ca+^{154}Sm (open circles) reactions.

following the same normalization procedure in the cross section estimates, the difference obtained seems to be noticeable. Of course, the detection of ER is an unambiguous signature of fusion since they can only come via the CN production in complete fusion but not via the QF process. The extraction of QF events (obtained with the simple cutting and Gaussian fitting procedures) has some uncertainty connected with the interference of QF with the deep-inelastic and quasielastic events. This procedure becomes more problematic in going to higher CN excitation energies. On the other hand one can suggest a "physical" reason of the observed discrepancy, implying that some part of CN-fission events belongs to QF, even if a "right" variance of the mass distributions and symmetric mass-angular distributions are observed. Such explanation looks quite reasonable, since an equilibration and the corresponding compact form at the saddle point do not mean that a system passed through the CN stage. Just as the absence of a forward-backward asymmetry does not exclude the presence of the QF component, since the observation of asymmetry relies only on the reaction time being comparable to the rotational period of the system. If, for instance, the reaction time for the QF process is substantially longer than the rotational period, this signature would be lost.

IV. SUMMARY

The mass-energy distributions of binary fission-like fragments produced in the reactions ^{16}O+^{186}W, ^{40}Ca+^{154}Sm and ^{48}Ca+^{144,154}Sm have been measured in the energy range from the Coulomb barrier to well above it, up to the excitation energy $E^*_{CN} = 100$ MeV. For all the reactions the main component of the distributions corresponds to a symmetrical mass division with typical values of the variance and mean total kinetic energies of fragments, which are inherent in CN fission.

For the ^{40,48}Ca+^{154}Sm reactions an asymmetric component in the fission-fragment mass distributions has been observed. The analysis of mass-energy distributions for these asymmetric "shoulders" points at the quasifission (QF) nature of this component. These QF "shoulders" peak around the masses having closed shells numbers of protons and neutrons. In the case of the ^{48}Ca reaction, the major part of the asymmetric component fits into the region of shells with $Z_L = 28$ and $N_H = 82$ for the light and heavy fragments, respectively. In the case of the ^{40}Ca reaction, the role of closed shells with $Z_L = 28$ and $Z_H = 50$ is less prominent in the formation of the QF asymmetric component. The contribution of the QF component to the total mass distribution of fission fragments increases, with respect to the symmetric CN-fission, as the projectile energy of ^{40,48}Ca decreases.

The mass-angular distributions obtained for the ^{48}Ca+^{154}Sm reaction support the QF nature of the asymmetric component. Preferential forward-peaking of the light-mass fission-fragments ($A_L = 73$–82) demonstrates that QF bypass the CN stage and occurs in time scales shorter than the rotational period for the ^{202}Pb*. This leads to a broken forward-backward symmetry of the angular distribution in the c.m. system for the asymmetric masses of fission fragments. In contrast to ^{48}Ca+^{154}Sm, symmetric angular distributions for all masses of fission fragments are clearly observed in the ^{48}Ca+^{144}Sm reaction. In the last case a CN nature of fission fragments is implied, i.e., one can state that the projectile-target system leading to ^{192}Pb* lives so long that is enough for several rotations. As the system rotates, it "forgets" entrance-channel conditions of its formation, i.e., moves to the CN production.

Thus in the ^{48}Ca+^{144}Sm reaction, no evidence of QF was found at the same CN excitation energy and angular momentum as in the case of the reaction with ^{154}Sm, where QF shows up. A small QF component has been also detected in the ^{40}Ca+^{154}Sm reaction at energies close to the Coulomb barrier. So, the QF effect is manifested in the reactions with the deformed target nucleus ^{154}Sm, which correspond to greater values of the entrance-channel mass-asymmetry than in the case of the ^{48}Ca reaction with spherical ^{144}Sm.

In contrast to the ER production in ^{48}Ca+^{154}Sm, which is strongly (by $\simeq 40\%$) suppressed (due to the QF effect, as one can reasonably propose) in a whole energy region measured above the Bass barrier [14], in the fission study QF is unambiguously observed at the level of $\lesssim 20\%$ at energies $\lesssim (B_{Bass} + 20)$ MeV. This discrepancy means that, from the experimental point of view, the imposed restrictions on the observable values in the fission experiment (the variance of the mass distribution, total kinetic energy and symmetry in the angular distribution) should be supplemented by some additional quantities for an unambiguous separation of CN fission and QF processes. From the point of view of theory, information on the mass and mass-angular distributions of products resulting from QF processes is earnestly required.

ACKNOWLEDGMENTS

We wish to thank the XTU Tandem staff for their careful work. The work was supported by the Russian Foundation for Basic Research (Grant No. 03-02-16779).

[1] R. Bock *et al.*, Nucl. Phys. **A388**, 334 (1982).
[2] J. Tōke *et al.*, Nucl. Phys. **A440**, 327 (1985).
[3] B. B. Back, Phys. Rev. C **31**, 2104 (1985).
[4] W. Q. Shen, J. Albinski, A. Gobbi, S. Gralla, K. D. Hildenbrand, N. Herrmann, J. Kuzminski, W. F. J. Muller, H. Stelzer, J. Toke, B. B. Back, S. Bjornholm, and S. P. Sorensen, Phys. Rev. C **36**, 115 (1987).
[5] D. J. Hinde, M. Dasgupta, J. R. Leigh, J. C. Mein, C. R. Morton, J. O. Newton, and H. Timmers, Phys. Rev. C **53**, 1290 (1996).
[6] J. C. Mein, D. J. Hinde, M. Dasgupta, J. R. Leigh, J. O. Newton, and H. Timmers, Phys. Rev. C **55**, R995 (1997).
[7] A. C. Berriman, D. J. Hinde, M. Dasgupta, C. R. Morton, R. D. Butt, and J. O. Newton, Nature (London) **413**, 144 (2001); D. J. Hinde, A. C. Berriman, R. D. Butt, M. Dasgupta, I. I. Gontchar, C. R. Morton, A. Mukherjee, and J. O. Newton, J. Nucl. Radiochem. Sci. **3**, 31 (2002).
[8] A. Y. Chizhov, M. G. Itkis, I. M. Itkis, G. N. Kniajeva, E. M. Kozulin, N. A. Kondratiev, I. V. Pokrovsky, R. N. Sagaidak,

V. M. Voskressensky, A. V. Yeremin, L. Corradi, A. Gadea, A. Latina, A. M. Stefanini, S. Szilner, M. Trotta, A. M. Vinodkumar, S. Beghini, G. Montagnoli, F. Scarlassara, A. Y. Rusanov, F. Hanappe, O. Dorvaux, N. Rowley, and L. Stuttge, Phys. Rev. C **67**, 011603(R) (2003).

[9] R. N. Sagaidak, G. N. Kniajeva, I. M. Itkis, M. G. Itkis, N. A. Kondratiev, E. M. Kozulin, I. V. Pokrovsky, A. I. Svirikhin, V. M. Voskressensky, A. V. Yeremin, L. Corradi, A. Gadea, A. Latina, A. M. Stefanini, S. Szilner, M. Trotta, A. M. Vinodkumar, S. Beghini, G. Montagnoli, F. Scarlassara, D. Ackermann, F. Hanappe, N. Rowley, and L. Stuttge, Phys. Rev. C **68**, 014603 (2003).

[10] M. G. Itkis *et al*., in *Proceedings of the 8th International Conference on Nucleus-Nucleus Collisions (NN2003), Moscow, 2003*, edited by Yu. Oganessian and R. Kalpakchieva [Nucl. Phys. **A734**, 136 (2004)].

[11] K. Lützenkirchen, J. V. Kratz, G. Wirth, W. Brüchle, K. Sümmerer, R. Lucas, J. Poitou, and C. Grégoire, Nucl. Phys. **A342**, 451 (1986).

[12] H. Keller, K. Lützenkirchen, J. V. Kratz, W. Brüchle, and K. Sümmerer, Z. Phys. A **326**, 313 (1987).

[13] B. B. Back, P. B. Fernandez, B. G. Glagola, D. Henderson, S. Kaufman, J. G. Keller, S. J. Sanders, F. Videbæk, T. F. Wang, and B. D. Wilkins, Phys. Rev. C **53**, 1734 (1996).

[14] A. M. Stefanini *et al*., Eur. Phys. J. A **23**, 473 (2005).

[15] C. E. Bemis, Jr., *et al*., ORNL Physics Division Progress Report 1986, ORNL-6326, p. 110.

[16] R. C. Lemmon, J. R. Leigh, J. X. Wei, C. R. Morton, D. J. Hinde, J. O. Newton, J. C. Mein, M. Dasgupta, and N. Rowley, Phys. Lett. **B316**, 32 (1993).

[17] R. J. Charity, J. R. Leigh, J. J. M. Bokhorst, A. Chatterjee, G. S. Foote, D. J. Hinde, J. O. Newton, S. Ogaza, and D. Ward, Nucl. Phys. **A457**, 441 (1986).

[18] D. J. Hinde, J. R. Leigh, J. O. Newton, W. Galster, and S. Sie, Nucl. Phys. **A385**, 109 (1982).

[19] R. N. Sagaidak *et al*., in *Proceedings of the 10th International Conference on Nuclear Reaction Mechanisms, Varenna, Italy, 2003*, edited by E. Gadioli (Universitá degli Studi di Milano, Milan, 2003), p. 301.

[20] R. Bass, Phys. Rev. Lett. **39**, 265 (1977); Lect. Notes Phys. **117**, 281 (1980).

[21] S. Raman, C. W. Nestor Jr., and P. Tikkanen, At. Data Nucl. Data Tables **78**, 1 (2001).

[22] A. J. Sierk, Phys. Rev. C **33**, 2039 (1986).

[23] V. E. Viola, K. Kwiatkowski, and M. Walker, Phys. Rev. C **31**, 1550 (1985).

[24] N. A. Kondratiev, E. M. Kozulin, I. V. Pokrovski, and E. V. Prokhorova, in *Proceedings of the 4th International Conference on Dynamical Aspects of Nuclear Fission, Častá-Papiernička, 1998*, edited by Yu. Ts. Oganessian *et al*., (World Scientific, Singapore, 2000), p. 431.

[25] I. V. Pokrovsky, L. Calabretta, M. G. Itkis, N. A. Kondratiev, E. M. Kozulin, C. Maiolino, E. V. Prokhorova, A.Ya. Rusanov, and S. P. Tretyakova, Phys. Rev. C **60**, 041304(R) (1999).

[26] G. Audi, A. H. Wapstra, and C. Thibault, Nucl. Phys. **A729**, 337 (2003).

[27] K. Hagino, N. Rowley, and A. T. Kruppa, Comput. Phys. Commun. **123**, 143 (1999).

[28] J. R. Nix and W. J. Swiatecki, Nucl. Phys. **71**, 1 (1965); J. R. Nix, Nucl. Phys. **A130**, 241 (1969).

[29] G. D. Adeev, I. I. Gonchar, V. V. Pashkevich, N. I. Pischasov, and O. I. Serdyuk, Fiz. Elem. Chastits At. Yadra **19**, 1229 (1988) [Sov. J. Part. Nucl. **19**, 529 (1988)]; G. D. Adeev and V. V. Pashkevich, Nucl. Phys. **A502**, 405 (1989).

[30] A. V. Ignatuk and I. N. Mikhailov, Communication of JINR, P4-12399, Dubna, 1979.

[31] G. G. Chubarian, M. G. Itkis, S. M. Lukyanov, V. N. Okolovich, Yu. E. Penionzhkevich, A.Ya. Rusanov, V. S. Salamatin, and G. N. Smirenkin, Yad. Fiz. **56**, 3 (1993).

[32] M. G. Itkis and A.Ya. Rusanov, Fiz. Elem. Chastits At. Yadra **29**, 389 (1998) [Phys. Part. Nucl. **29**, 160 (1998)].

[33] S. Cohen, F. Plasil, and W. J. Swiatecki, Ann. Phys. (NY) **82**, 557 (1974).

[34] I. Halpern and V. M. Strutinski, in *Proceedings of the Second United Nations International Conference on the Peaceful Uses Of Atomic Energy, Geneva, Swizerland, 1957* (United Nations, Geneva, Switzerland, 1958), p. 408.

[35] A. Diaz-Torres, G. G. Adamian, N. V. Antonenko, and W. Scheid, Nucl. Phys. **A679**, 410 (2001); Phys. Rev. C **64**, 024604 (2001).

[36] V. I. Zagrebaev, Phys. Rev. C **64**, 034606 (2001).

[37] G. Royer and B. Remaud, Nucl. Phys. **A444**, 477 (1985).

[38] R. Moustabchir and G. Royer, Nucl. Phys. **A683**, 266 (2001).

[39] P. Möller, J. R. Nix, W. D. Myers, and W. J. Swiatecki, At. Data Nucl. Data Tables **59**, 185 (1995).

[40] R. N. Sagaidak *et al*., in *Proceedings of the 11th International Conference on Nuclear Reaction Mechanisms, Varenna, Italy, 2006*, edited by E. Gadioli (Universitá degli Studi di Milano, Milan, 2006), p. 279.

[41] V. I. Zagrebaev *et al*., OM code of NRV, http://nrv.jinr.ru/nrv/.

[42] C. Y. Wong, Phys. Lett. **B26**, 120 (1968); L. Wilets, E. Guth, and J. S. Tenn, Phys. Rev. **156**, 1349 (1967); H. Holm, W. Scheid, and W. Greiner, Phys. Lett. **B29**, 473 (1969); H. Holm and W. Greiner, Phys. Rev. Lett. **24**, 404 (1970); A. S. Jensen and C. W. Wong, Phys. Rev. C **1**, 1321 (1970).